Fission Properties of Neutron-Rich Nuclei around the End Point of *r*-Process

Jiawei Chen(陈佳炜), Junchen Pei(裴俊琛)*, Yu Qiang(强雨), and Jihuai Chi(迟济怀)

State Key Laboratory of Nuclear Physics and Technology, School of Physics, Peking University, Beijing 100871, China

(Received 10 October 2022; accepted manuscript online 30 November 2022)

We studied the fission properties of neutron-rich nuclei ^{278,286}Cf around the end point of r-process by microscopic self-consistent approaches. The fission barriers and potential energy surfaces are obtained by constrained static Skyrme Hartree–Fock-BCS calculations. Fission fragments are studied by dynamical time-dependent Hartree–Fock+BCS calculations. Results show that ^{286}Cf has an octupole deformation at ground state, which can increase the fission barrier height by 1.1 MeV and enhance significantly the spontaneous fission half-life. To search possible fission channels, dynamical calculations with a broad coverage of initial deformations result in two slightly asymmetric peaks around $A = 128$ and 150 for ^{278}Cf, and $A = 133$ and 153 for ^{286}Cf. Very asymmetric fission channels as given by semi-empirical models are not found in our results.

DOI: 10.1088/0256-307X/40/01/012401

The recent observation of gravitational wave event GW170817 from the binary neutron star merger has attracted great interests in nuclear astrophysics.[1] Following the GW170817 event, the kilonova electromagnetic transient was observed, resulting from the ejection of ~ 0.05 solar masses of neutron-rich material,[2] which is an evidence of rapid neutron capture process (r-process). The ejecta from core collapse supernova (CCSN) is also a possible scenario for r-process. The r-process involving high neutron flux is responsible for producing half of the elements heavier than iron and all elements beyond bismuth.

The r-process would be terminated in the neutron-rich superheavy region due to fission and rarely goes beyond the element $Z = 100$.[3,4] The consequent fission fragments would be recycled in the r-process and impact the final element abundances significantly.[5,6] The neutrons and heat generated from fission also affect the r-process observations.[7] The importance of fission in r-process is well established, and fission is one of the main sources of uncertainties in r-process simulations. The uncertainties of nuclear inputs are also related to pin down the r-process environments.[8] The problem is to develop reliable theoretical models for descriptions of fission in these extremely neutron-rich nuclei, since it is impossible to access this region experimentally.

Conventionally the fission properties for r-process simulations are given by semi-empirical models.[3] For example, the statical scission-point model SPY calculates fission fragment distributions by considering the deformed fragment configurations at scission.[3] GEF is a well-known comprehensive phenomenological model to calculate various fission observables,[9] by taking into account shell structures, level densities, energy dependence and fission barriers with many parameters. These phenomenological models can well describe existing fission data but are questionable when being extrapolated to unknown regions.

The microscopic studies of fission are now promising with the developments of supercomputing capabilities. The density functional theory is the suitable choice for microscopic self-consistent calculations of heavy and superheavy nuclei since *ab initio* studies of fission are practically impossible. The self-consistent calculations based on effective nuclear forces are free of parameters and can in principle provide most reliable fission properties of inaccessible nuclear regions. The time-dependent generate-coordinate method (TD-GCM) based on microscopic potential energy surface (PES) can reasonably describe the distributions of fission fragment yields.[10,11] TD-GCM is an adiabatic approach on static PES and is unsuitable for descriptions of excitations of fragments and released energies. The accuracy of TD-GCM largely relies on the quality of multi-dimensional PES. Nevertheless, TD-GCM studies of fission in the r-process region are unavailable yet. Similarly the fission fragment yields can be calculated by the Langevin equation on the macroscopic-microscopic PES.[12,13] The time-dependent density functional theory (TD-DFT) is suitable for studying fission mechanism and multiple fission observables.[14–17] Within TD-DFT, the distributions of fission observable are narrow and fluctuations are needed.[16] To our knowledge, TD-DFT has not been applied to study fission of r-process nuclei. There are large discrepancies[3] in the fission observables of the r-process nuclei by various phenomenological models and microscopic studies are desirable.

Our main aim of this work is to study the fission barriers and fission fragments using microscopic self-consistent methods for the r-process nuclei. The r-process is possible to produce neutron-rich superheavy nuclei up to $Z = 100$ and cross the $N = 184$ neutron shell if neutron flux is sufficiently high. The region with nuclear mass $A < 292$ and neutron number $N > 184$ is predicted to be the fission bottleneck.[3,4] A special case is ^{278}Cf whose fission yields are important to explain the r-process peak around $A = 165$ with two very asymmetric fission channels.[6] Re-

*Corresponding author. Email: peij@pku.edu.cn
© 2023 Chinese Physical Society and IOP Publishing Ltd

cently the updated results from this group show that the peak of fission yields around $A = 165$ disappears.[3] Different models show large discrepancies in distributions of fission yields in ^{278}Cf.[3] Presently we like to focus on the fission properties of ^{278}Cf and the more neutron-rich isotope ^{286}Cf in the bottleneck, since systematic microscopic calculations are too expensive.

In this work, the fission barriers and PES are obtained by deformation constrained Skyrme–Hartree–Fock+BCS calculations.[18] The quadrupole deformation β_2 and the octupole deformation β_3 are adopted in the two-dimensional constrained calculations.

$$H_c = H - \lambda_l(\langle\beta_l\rangle - \beta_l^c), \tag{1}$$

where H denotes the single-particle Hamiltonian; λ_l denotes the Lagrangian multiplier for the corresponding multipole constraint; β_l^c denotes the multipole deformation to be constrained. The nuclear interaction SkM*[19] and the mixed pairing interaction[20] are used. In the mixed pairing, a mixing factor of 0.5 is used.[20] The pairing strengths are taken as 456 and 427 MeV·fm^3 for protons and neutrons, respectively. The same pairing interaction is used in both static and dynamical calculations. Note that SkM* is particularly fitted for descriptions of fission barriers. The Hartree–Fock equation is iteratively solved by the SkyAX code in the cylindrical lattice space.[21] Based on fission barriers, the spontaneous fission half-lives can be calculated with the WKB approximation.[22] The fission width Γ along the fission pathway s can be calculated by $\Gamma = P/F$ as[22]

$$P = \left[1 + \exp\left(2\int_b^c \sqrt{2M(s)(V(s) - E_0)}ds\right)\right]^{-1}, \tag{2a}$$

$$F = \int_a^b ds\left(\sqrt{\frac{(E_0 - V(s))}{2M(s)}}\right)^{-1}, \tag{2b}$$

where the fission barrier $V(s)$ is given by SHF-BCS calculations; a, b, and c are the tunneling points associated WKB calculations.[22] The collective mass parameter $M(s)$ is given by the cranking approximation.[22] The fission lifetime is given by $\hbar/\Gamma$.

With the initial wavefunctions obtained by constrained calculations, the dynamical fission evolutions are described by the time-dependent Skyrme–Hartree–Fock+BCS (TD-BCS) approach.[16] The framework of time-dependent HF-BCS is similar to the time-dependent Hartree–Fock–Bogoliubov (HFB) formulism:[23]

$$i\hbar\frac{\mathrm{d}\mathcal{R}}{\mathrm{d}t} = [H, \mathcal{R}], \tag{3}$$

where H is the HFB hamiltonian; $\mathcal{R}$ is the general density matrix. The TD-BCS equations can be derived by using BCS basis or canonical basis.[23] Note that TD-BCS can describe dynamical pairing approximately compared to the fully dynamical pairing in TD-HFB. TD-BCS calculations are performed with the Sky3D code.[24] The time step in this work is 0.15 fm/c. It must be noted that pairing is essential for descriptions of fission dynamics. The fission fragments and total kinetic energy from TD-BCS are not correct without pairing.[16]

Figure 1 shows the fission barriers of ^{278}Cf and ^{286}Cf as a function of quadrupole deformation β_2. The asymmetric fission has been taken into account. The quadrupole deformation β_2 is close to zero in the ground states of both nuclei. For ^{278}Cf, we see that the second fission barrier is considerable, which is about 7.3 MeV. The calculated spontaneous fission half-life is 5.9×10^7 s. For ^{286}Cf, its fission barrier becomes lower compared to that of ^{278}Cf. In the symmetric fission mode, the second fission barrier is about 3.7 MeV. However, the ground state of ^{286}Cf has an octupole deformation, which adds extra binding energies and the fission barrier height is increased to 4.8 MeV. The calculated spontaneous fission half-lives are 3.9×10^7 s with octupole deformation and 2.9×10^3 s without octupole deformation. Note that the theoretical spontaneous fission half-lives are also dependent on the approaches in calculating collective inertia of mass. It has been known that the octupole deformation can reduce the second fission barriers of actinide nuclei[25,26] and superheavy nuclei.[27] In our case, the ground state of ^{286}Cf has an octupole deformation while it is nearly spherical. The increased fission barrier due to octupole deformation is significant in enhancing spontaneous fission half-lives. The existence of octupole deformation at ground states in this region provides an optimistic reason that r-process could go further than being expected. It is worth to revisit the long standing question that if superheavy nuclei can be produced by r-process.[1] In spite of the ground-state deformations, the symmetric and asymmetric fission barrier are the same up to $\beta_2 = 1.5$. This means that the symmetric fission mode is dominated in both nuclei.

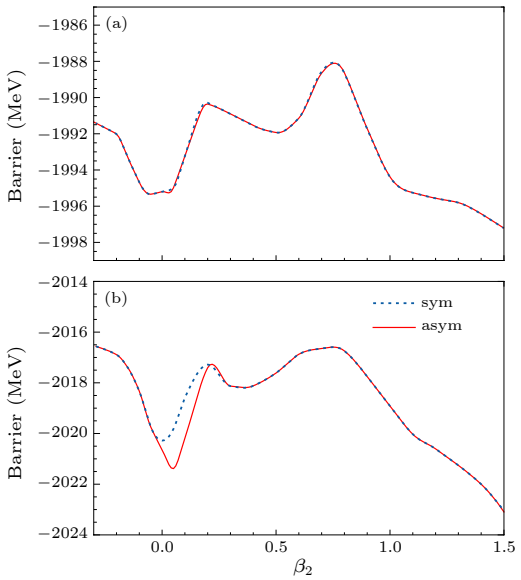

Fig. 1. Fission barriers obtained by constrained SHF-BCS calculations for ^{278}Cf (a) and ^{286}Cf (b). Fission barriers along symmetric and asymmetric fission pathways are shown.

To explore possible asymmetric fission channels, the real-time TD-BCS calculations are performed with different initial deformations. The fission pathways are shown in Fig. 2. It is known that TD-BCS calculations cannot produce sufficient spreading fission observables,[14] but are

good to reproduce the averaged fission fragment mass and total kinetic energies, as demonstrated in the fission properties of ^{240}Pu.[16] Without fluctuations, TD-BCS would result in the most probable fission channel. In this case, we adopt a very broad coverage of initial deformations, so that very asymmetric fission channels would not be missed.

Table 1. The TD-BCS calculated fission fragments and total kinetic energies (TKE) (in MeV) of ^{278}Cf and ^{286}Cf. The dynamical evolutions are performed with different initial deformations (β_2, β_3, β_4). The evolution time is given in fm/c. The proton number, neutron numbers and total mass A of the light and heavy fragments are listed.

β_2	β_3	β_4(initial)	β_4	Time	N_H	Z_H	N_L	Z_L	A_H	A_L	TKE
^{278}Cf											
2.5	1.4	5.4	5.3	6354	98.49	53.27	81.31	44.73	151.75	126.04	173
2.5	1	4.8	4.8	3306	97.09	53.11	82.87	44.89	150.18	127.76	167
2.7	0.8	5.4	5.4	8886	95.55	51.75	84.38	46.25	147.29	130.63	174
3	0.6	5.6	5.6	744	91.11	48.95	88.88	49.05	140.06	137.93	175
3.5	0.2	8.5	9.7	850	89.99	49.47	89.99	48.53	139.47	138.51	164
^{286}Cf											
2.5	1.4	4.8	5.3	4516	100.86	52.92	86.88	45.08	153.78	131.97	176
2.5	1	4.3	4.9	9046	100.98	52.75	86.60	45.25	153.74	131.84	174
2.7	0.8	5	5.5	8178	99.84	52.30	87.91	45.70	152.13	133.62	174
3	0.6	5.7	6.3	1008	98.13	51.85	89.84	46.15	149.98	135.99	177
3.5	0.2	8.8	9.6	5410	95.57	49.85	92.34	48.15	145.42	140.49	164

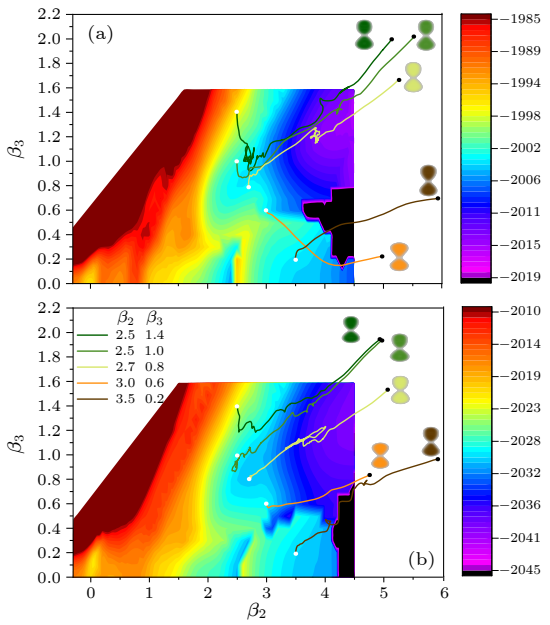

Fig. 2. The TD-BCS calculated dynamical fission trajectories of ^{278}Cf (a) and ^{286}Cf (b), corresponding to Table 1. The associated potential energy surfaces are also shown.

The detailed results of dynamical fission evolutions are listed in Table 1. Note that in this neutron-rich superheavy region, the fission dynamics are strongly dissipated and hindered. There are some events that have lots of fluctuations in pathways as shown in Fig. 2, indicating strong dissipations. This can be understood that the role of Coulomb potential as the fission driving force is reduced in extremely neutron-rich nuclei, and consequently the fission dynamics would be hindered. Thus, in practical dynamical calculations, the initial hexadecapole deformation β_4 is also slightly changed, while β_2 and β_3 are constrained. Otherwise, the dynamical evolution would be difficult to reach the scission. This is similar to the deformation-induced fission.[28] For ^{278}Cf, the asymmetric peaks are around $A = 128$ and 150, respectively. There are also two events close to the symmetric channel. The 5th event has a larger final octupole deformation than that of 4th event, but has a slightly smaller asymmetry between fragments. This is because the shape of the 5th event is more elongated. For ^{286}Cf, we can see that the fission yields are mainly distributed around two peaks. The asymmetric channel corresponds to $A = 133$ and 153. For ^{278}Cf and ^{286}Cf, the allocation of proton numbers in two fragments is similar. The obtained TKEs are in the range of 164 MeV to 177 MeV, which are not very different from the actinide nucleus ^{240}Pu.[16] According to the PES, although some events have very large initial octupole deformations, the results have not any events with fragments around $A = 165$.

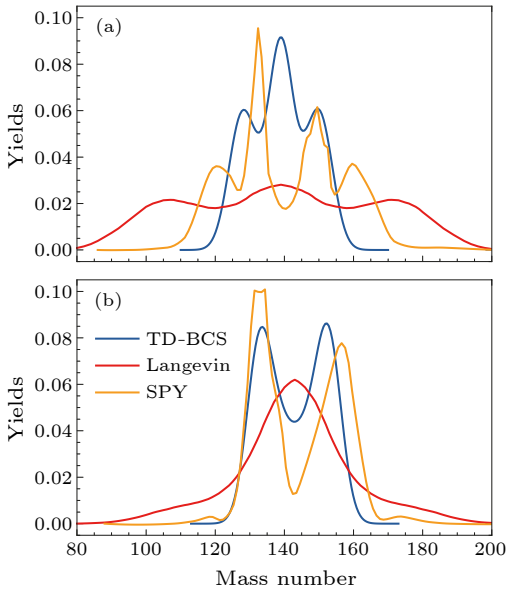

Fig. 3. The smoothed fission yields from TD-BCS calculations for ^{278}Cf (a) and ^{286}Cf (b). The results from the Langevin equation are also shown for comparison.[13] The recent SPY fission yields are taken from Ref. [3].

The distributions of fission fragment yields from dynamical calculations are displayed in Fig. 3. The obtained

fission yields are smoothed for comparison with other models. The fission yields are smoothed by the Gaussian function with a width of 3.5. Note that our aim of TD-BCS calculations is to explore possible fission channels, not to provide complete realistic fission yields which need very costly calculations. The distributions range from $A = 110$ to 155, and dynamical fission channels are slightly asymmetric. The TD-BCS evolution is not dependent on the details of PES. In the Langevin model, the fission yields range from $A = 95$ to 185 for ^{278}Cf.[13] For ^{286}Cf by the Langevin model, the fission channel is symmetric with a distribution from $A = 130$ to 155.[13] In the GEF model, fission channels of both nuclei are very asymmetric.[3] In the recent SPY model based on microscopic PES, the fission channels in ^{278}Cf and^{286}Cf are slightly asymmetric,[3] which are similar to our dynamical results.

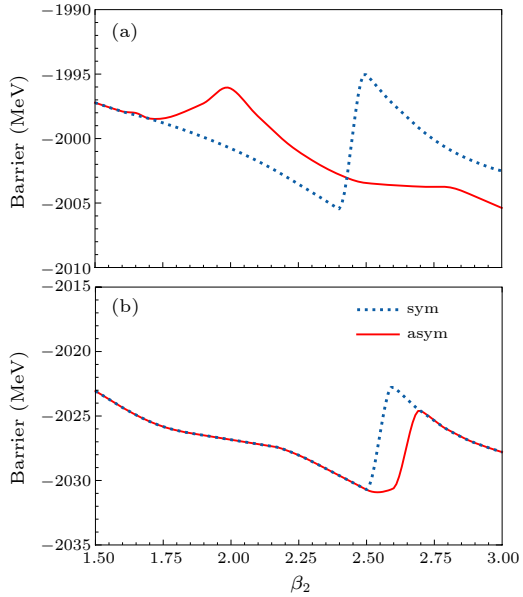

Fig. 4. The calculated fission barriers of ^{278}Cf (a) and ^{286}Cf (b) at large deformations with β_2 from 1.5 to 3.0. Both symmetric and asymmetric fission pathways are shown.

Figure 4 displays the fission barriers at large deformations with $\beta_2 > 1.5$, which is related to the later part of fission dynamics. The fission barriers shown in Fig. 1 is mainly related to the spontaneous fission. We see that there is a third barrier at large deformations. The third minima and barrier have been discussed in actinide nuclei and they are related to complex structures of single-particle levels.[29] For ^{278}Cf, the third asymmetric fission barrier is lower than the symmetric case by 1 MeV. The third barrier is around −1995 MeV, which is slightly higher than the ground state energy. This could affect the spontaneous fission properties, but the thermal neutron induced fission would not be affected. For ^{286}Cf, the third symmetric and asymmetric fission barriers are similar, and both are lower than the ground state energy, which means that spontaneous and induced fissions are not much affected by the third barrier. The comprehensive studies reveal that symmetric fission channels are dominated in both ^{278}Cf and ^{286}Cf according to fission barriers in Figs. 1, 2, and 4. Moreover, there are some additional slightly asymmetric fission yields from dynamical evolutions as shown in Fig. 3. Our results show that the assumption of symmetric fission adopted by the REACLIB library[30] is approximately valid for these end-point nuclei of r-process. The calculated neutron separation energies in ^{278}Cf and ^{286}Cf using SkM* force are 4.2 and 2.48 MeV, respectively, which are smaller than their fission barrier heights as shown in Fig. 1. This means that r-process can survive the thermal neutron induced fission across the $N = 184$ shell for Cf isotopes.

In summary, we have performed the microscopic studies of fission properties of neutron-rich nuclei ^{278,286}Cf, which are around the end point of r-process. The fission barriers and spontaneous fission half-lives are obtained based on static constrained Skyrme Hartree–Fock-BCS calculations. The fission fragments are studied by the time-dependent Skyrme Hartree–Fock+BCS method, which is suitable for descriptions of averaged fission observables. To our knowledge, the microscopic studies of fission dynamics of this region are unavailable before. There are some insights obtained in this work.

(1) The ground state of ^{286}Cf has an octupole deformation, which can increase its fission barrier height by 1.1 MeV and its spontaneous fission half-life by 4 orders. This is favorable for the r-process across the $N = 184$ shell.

(2) The symmetric fission channels are dominated in ^{278,286}Cf according to the PES and fission barriers, and additional slightly asymmetric fission yields are also presented from dynamical evolutions. This indicates that the assumption of symmetric fission in the REACLIB library[30] is approximately valid.

(3) Very asymmetric fission channels given by semi-empirical models are not found in this work, as searched by dynamical evolutions with a broad coverage of initial deformations. This means the earlier claim[6] that the origin of the r-process peak at $A = 165$ is due to fission needs to be reconsidered. In the future, we aim to develop a comprehensive and predictable fission theory and perform systematic calculations for the r-process nuclei.

Acknowledgments. This work was supported by the National Key R&D Program of China (Grant No. 2018YFA0404403), and the National Natural Science Foundation of China (Grant Nos. 11975032, 11835001, 11790325, and 11961141003).

References

[1] Cowan J J, Sneden C, Lawler J E, Aprahamian A, Wiescher M, Langanke K, Martínez-Pinedo G, and Thielemann F K 2021 *Rev. Mod. Phys.* **93** 015002

[2] Drout M R 2017 *Science* **358** 1570

[3] Lemaitre J F, Goriely S, Bauswein A, and Janka H T 2021 *Phys. Rev. C* **103** 025806

[4] Giuliani S A, Martinez-Pinedo G, and Robledo L M 2018 *Phys. Rev. C* **97** 034323

[5] Eichler M, Arcones A, Kelic A, Korobkin O, Langanke K, Marketin T, Martinez-Pinedo G, Panov I, Rauscher T, Rosswog S, Winteler C, Zinner N T, and Thielemann F K 2015 *Astrophys. J.* **808** 30

[6] Goriely S, Sida J L, Lemaître J F, Panebianco S, Dubray N, Hilaire S, Bauswein A, and Janka H T 2013 *Phys. Rev. Lett.* **111** 242502

[7] Zhu Y L, Lund K A, Barnes J, Sprouse T M, Vassh N, McLaughlin G C, Mumpower M R, and Surman R 2021 *Astrophys. J.* **906** 94

[8] Chai Q Z, Qiang Y, and Pei J C 2022 *Phys. Rev. C* **105** 034315

[9] Schmidt K H, Jurado B, Amouroux C, and Schmitt C 2016 *Nucl. Data Sheets* **131** 107

[10] Regnier D, Dubray N, Schunck N, and Verriere M 2016 *Phys. Rev. C* **93** 054611

[11] Zhao J, Nikšić T, Vretenar D, and Zhou S G 2019 *Phys. Rev. C* **99** 014618

[12] Liu L L, Wu X Z, Chen Y J, Shen C W, Li Z X, and Ge Z G 2019 *Phys. Rev. C* **99** 044614

[13] Mumpower M R, Jaffk P, Verriere M, and Randrup J 2020 *Phys. Rev. C* **101** 054607

[14] Bulgac A, Jin S, Roche K J, Schunck N, and Stetcu I 2019 *Phys. Rev. C* **100** 034615

[15] Scamps G, Simenel C, and Lacroix D 2015 *Phys. Rev. C* **92** 011602(R)

[16] Qiang Y, Pei J C, and Stevenson P D 2021 *Phys. Rev. C* **103** L031304

[17] Qiang Y and Pei J C 2021 *Phys. Rev. C* **104** 054604

[18] Ring P and Schuck P 2004 *The Nuclear Many-Body Problem* (Berlin: Springer)

[19] Bartel J, Quentin P, Brack M, Guet C, and Håkansson H B 1982 *Nucl. Phys. A* **386** 79

[20] Dobaczewski J, Nazarewicz W, and Stoitsov M V 2002 *Eur. Phys. J. A* **15** 21

[21] Reinhard P G, Schuetrumpf B, and Maruhn J A 2021 *Comput. Phys. Commun.* **258** 107603

[22] Zhu Y and Pei J C 2016 *Phys. Rev. C* **94** 024329

[23] Ebata S, Nakatsukasa T, Inakura T, Yoshida K, Hashimoto Y, and Yabana K 2010 *Phys. Rev. C* **82** 034306

[24] Maruhn J A, Reinhard P G, Stevenson P D, and Umar A S 2014 *Comp. Phys. Comm.* **185** 2195

[25] Lu B N, Zhao E G, and Zhou S G 2012 *Phys. Rev. C* **85** 011301(R)

[26] Lu B N, Zhao J, Zhao E G, and Zhou S G 2014 *Phys. Rev. C* **89** 014323

[27] Meng X, Lu B N, and Zhou S G 2020 *Sci. Chin. Phys. Mech. Astron.* **63** 212011

[28] Goddard P, Stevenson P, and Rios A 2015 *Phys. Rev. C* **92** 054610

[29] Zhao J, Lu B N, Vretenar D, Zhao E G, and Zhou S G 2015 *Phys. Rev. C* **91** 014321

[30] Cyburt R H, Amthor A M, Ferguson R, Meisel Z, Smith K, Warren S, Heger A, Hoffman R D, Rauscher T, Sakharuk A, Schatz H, Thielemann F K, and Wiescher M 2010 *Astrophys. J. Suppl. Ser.* **189** 240